JETIR.ORG ISSN: 2349-5162 | ESTD Year : 2014 | Monthly Issue
JOURNAL OF EMERGING TECHNOLOGIES AND INNOVATIVE RESEARCH (JETIR)
An International Scholarly Open Access, Peer-reviewed, Refereed Journal

Modelling and Comparative Analysis of Series- and Parallel-Connected Coupled-Inductor Boost Converters

Smitha Joseph
Lecturer in Electrical &Electronics Engineering,
Government Polytechnic College, Kalamassery, Kerala, India.

Abstract : This paper presents the modelling and comparison of two non-isolated high step-up DC–DC converters based on a coupled inductor: a series-connected and a parallel-connected configuration. In both topologies, the conventional boost inductor is replaced by a coupled inductor with a controllable turns ratio, enabling higher conversion ratios without resorting to extreme duty cycles. To keep the model suitable for control design, the coupled inductor is represented by its magnetizing inductance, with parasitic effects included while leakage inductance is neglected. For each converter, a steady-state analysis in continuous conduction mode (CCM) is performed to obtain the voltage gain and semiconductor device stresses. A unified averaged state-space model is then derived, and linearized small-signal models are obtained for controller design. Simulation results in MATLAB/Simulink confirm the analytical predictions and highlight the main trade-offs between the series-connected and parallel-connected topologies.

Index Terms **- Coupled inductor, small signal modelling, magnetizing inductance, high step-up DC–DC converter**

I. INTRODUCTION

Many emerging applications, including low-voltage photovoltaic (PV) modules, fuel cells, and battery systems for electric vehicles, require efficient high step-up DC–DC conversion. The conventional boost converter is simple and widely used, but its performance deteriorates as the required voltage gain increases. To reach a large conversion ratio, the duty cycle must approach unity, which leads to high current stress, large conduction and switching losses, and poor dynamic behaviour.

Coupled-inductor topologies have been proposed as an effective way to enhance the voltage gain while maintaining a moderate duty cycle and continuous input current [1],[2]. By replacing the single boost inductor with a coupled inductor, the designer can exploit the turns ratio to extend the voltage gain and redistribute stresses. Among the many possible arrangements, two simple and attractive options are:

1. **Series-connected coupled-inductor boost converter**, where the primary and secondary windings contribute in series to the output during the energy transfer interval.
2. **Parallel-connected coupled-inductor boost converter**, where the windings share current in parallel in one interval and contribute differently in the other, reducing current ripple and device stress.

Small-signal models that include leakage inductance effects [3] and switching losses [4] have been reported in the literature. In this work, a small-signal model is derived that retains only the dominant parasitic elements, which are sufficient to capture the essential behavior of the system and accurately predict its dynamic response. Although detailed magnetic and parasitic models can be used, they often become cumbersome for control design. In this work, both converters are modelled in a simplified manner captures the essential dynamics needed to design a closed-loop controller and to compare their performance.

This paper is organized as follows. Section II describes the circuit configuration and operating principles of both the series- and parallel-connected coupled-inductor converters. The steady-state analysis is presented in Section III. Section IV addresses the linearized small-signal modelling, and Section V discusses the simulation and analytical results. Finally, Section VI provides the conclusions.

II. CIRCUIT DESCRIPTION AND OPERATING PRINCIPLE

2.1 Series-Connected Coupled-Inductor Boost Converter

In the series-connected topology in Fig. 1, the coupled inductor consists of a magnetizing inductance $L_m$and an ideal transformer with turns ratio $n = N_2/N_1$. The primary side is connected between the input source $V_{in}$and the switch node, while the secondary is arranged so that, during the off-state, the induced secondary voltage adds in series with the primary voltage toward the output through diode D. The output is filtered by capacitor $C$and supplies a resistive load R.

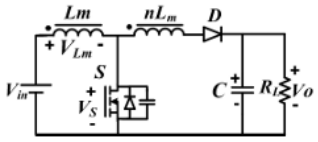

Fig.1 Series connected coupled inductor boost converter

Mode 1 (switch ON):

Figure 2(a) shows the ON period of series-connected CI boost converter. The main switch *S*conducts, diode *D*is reverse biased, and the magnetizing inductance is energized from the input. The load is supplied by the output capacitor.

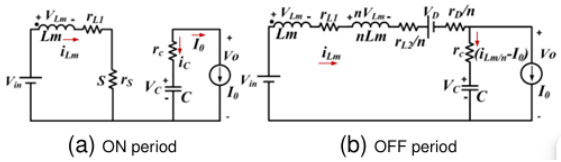

Fig.2 ON and OFF periods of series-connected CI boost converter

Mode 2 (switch OFF):

Figure 2(b) shows the OFF period of series-connected CI boost converter. The switch is turned off, diode *D*turns on, and the energy stored in $L_m$is transferred to the output. The primary and secondary voltages appear in series at the output, resulting in an increased effective boost action.

2.2 Parallel-Connected Coupled-Inductor Boost Converter

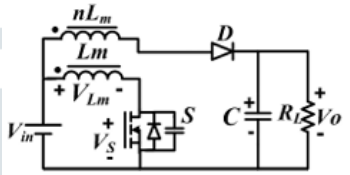

Fig.3 Parallel connected coupled inductor boost converter

In the parallel-connected topology in Fig. 3, the same coupled inductor is used, but the windings are rearranged so that they behave effectively in parallel from the input side in one interval and in a different configuration in the other interval. The goal is to share the input current between the windings and reduce current ripple and device stresses.

Mode 1 (switch ON):

Figure 4(a) shows the ON period of parallel-connected CI boost converter. The switch *S*conducts and both windings are energized in a way that they draw current from the source with a largely parallel effect, leading to reduced input current ripple.

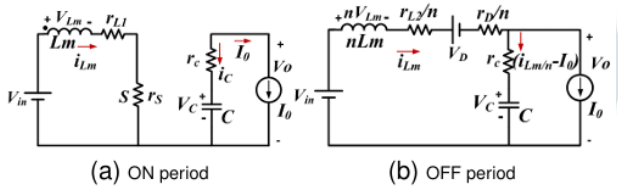

Fig.4 ON and OFF periods of Parallel connected coupled inductor boost converter

Mode 2 (switch OFF):

Figure 4(b) shows the ON period of parallel-connected CI boost converter. The energy stored in the magnetizing inductance is released to the load through diode *D*. The contribution of the secondary depends on the exact connection, but generally it partially assists the primary in boosting the output voltage, giving a gain higher than the conventional boost, though typically lower than the series-connected case for the same turns ratio.

III. Steady State Analysis

To obtain models suitable for analysis and control design, the following assumptions are introduced:

- The coupled inductor is represented by a magnetizing inductance L_m,and leakage inductances is neglected due its small value compared to magnetic inductance.
- The converter operates in continuous conduction mode (CCM), so the magnetizing current never falls to zero.
- The output capacitor *C*is large enough that the output voltage ripple is small within a switching period.

Under these assumptions, each topology can be described by two operating sub-intervals per switching period, and averaged over one period using standard state-space averaging.

Let *d*denote the duty cycle and $T_s$the switching period. Volt-second balance is applied to the magnetizing inductance L_m.

$$d\, v_{\{Lm,on\}} + (1 - d) v_{\{Lm,off\}} = 0 \quad (1)$$

The ideal voltage gain of series-connected CI boost converter is

$$Gain\_s = \frac{(1 + n\, d)}{(1 - d)} \quad (2)$$

The ideal voltage gain of parallel-connected CI boost converter is

$$Gain\_p = \frac{(1 + n\,d - d)}{(1 - d)} \tag{3}$$

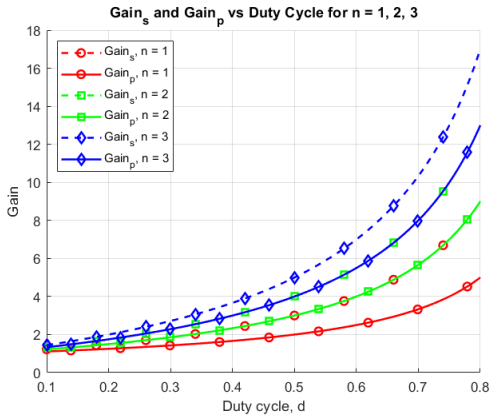

Fig. 5 Comparison of ideal voltage gain equations

Figure 5 illustrates these two gain characteristics as functions of the duty cycle for $n = 1,2,$and 3. The series-connected converter consistently exhibits a higher voltage gain than the parallel-connected one, highlighting its suitability for applications requiring very high step-up ratios. The parallel-connected topology, while offering a more modest gain, provides an appreciable improvement over the conventional boost converter and may be preferred when other factors such as current sharing and device stress are considered.

IV. Linearized Small Signal Modelling

Let r_{L1} and r_{L2} are the parasitic resistances of coupled inductor in primary and secondary sides, r_S is the switch resistance, r_C is the ESR of capacitor, r_D is the forward resistance of the diode and V_D is the cut-in voltage of the diode.

a) Linearized Small-Signal Model of Series connected Coupled Inductor Boost Converter

The inductor in the boost converter can now be replaced with a coupled inductor to enhance the voltage gain by taking advantage of its turns ratio. The primary and secondary windings of the coupled inductor is connected in series, as shown in Fig. 6.

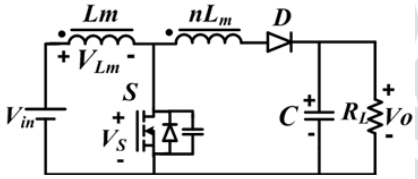

Fig. 6 Series connected coupled inductor boost converter

Consider the ON and OFF circuit configurations of the series-connected coupled inductor boost converter, including parasitic elements, as depicted in Fig. 7.

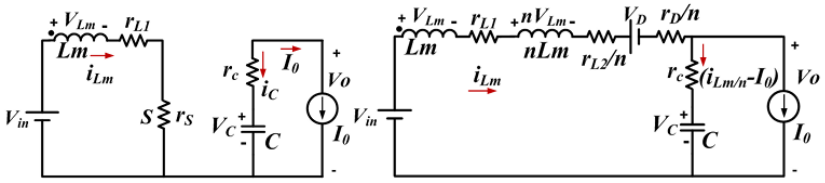

Fig. 7 ON and OFF periods of series connected coupled inductor boost converter

The primary inductance of the coupled inductor is denoted as *Lm*, while the secondary inductance is expressed as *nLm*, where *n* is the turns ratio of the coupled inductor. The independent state variables are the magnetizing inductance current, i_{Lm} and the voltage across the output capacitor, V_C. The state-space averaged model is derived by applying Kirchhoff's voltage and current laws to the ON and OFF circuit configurations. The ON-state equations are given below:

$$V_{LmON} = V_{in} - i_{Lm}\,(r_{L1} + r_S) \tag{4}$$

$$i_{CON} = -I_0 \tag{5}$$

$$V_0 = V_C - I_0 r_C \tag{6}$$

The OFF-state equations are given below:

$$(n+1)V_{LmOFF} = V_{in} - V_D - V_C + I_0 r_C - i_{Lm}\left(r_{L1} + \frac{r_{L2}}{n} + \frac{r_D}{n} + \frac{r_C}{n}\right) \tag{7}$$

$$i_{COFF} = \frac{i_{Lm}}{n} - I_0 \tag{8}$$

$$V_0 = V_C + \frac{i_{Lm} r_C}{n} - I_0 r_C \tag{9}$$

By applying the volt-second balance principle to the above equations, the ideal voltage gain of the series connected coupled inductor boost converter can be derived as follows.

$$V_0/V_{in} = (1 + nd)/(1 - d) \tag{10}$$

The ON period is identical to that of a conventional boost converter, while during the OFF period, the elements discharge in series to achieve a high voltage gain. The state equations are derived as presented in (11) and (12).

$$\begin{bmatrix} \frac{d\overline{i_{Lm}}}{dt} \\ \frac{d\overline{v_C}}{dt} \end{bmatrix} = \begin{bmatrix} -\left(\frac{d_0 r_{on}}{L_{on}} + \frac{(1-d_0) r_{off}}{L_{off}}\right) & -\frac{(1-d_0)}{L_{off}} \\ \frac{(1-d_0)}{nC} & 0 \end{bmatrix} \begin{bmatrix} \overline{i_{Lm}} \\ \overline{v_C} \end{bmatrix} + \begin{bmatrix} \frac{d_0}{L_{on}} + \frac{1-d_0}{L_{off}} & -\frac{(1-d_0)}{L_{off}} & \frac{(1-d_0) r_C}{L_{off}} \\ 0 & 0 & -\frac{1}{C} \end{bmatrix} \begin{bmatrix} \overline{v_{in}} \\ V_D \\ \overline{i_o} \end{bmatrix} \tag{11}$$

where $L_{on} = L_m, L_{off} = (n+1)L_m, r_o n = r_{L1} + r_s, r_{off} = r_{L1} + r_{L2}/n + r_D/n + r_C/n$

$$\bar{v}_o = \begin{bmatrix} (1-d_0)\frac{r_C}{n} & 1 \end{bmatrix} \begin{bmatrix} \overline{i_{Lm}} \\ \overline{v_C} \end{bmatrix} + \begin{bmatrix} 0 & 0 & -r_C \end{bmatrix} \begin{bmatrix} \overline{v_{in}} \\ V_D \\ \overline{i_o} \end{bmatrix} \tag{12}$$

$$\alpha \approx \frac{V_0}{L_{off}} \ , \ \gamma \approx 0 \tag{25}$$

$$\beta = \frac{-\text{Gain}.I_0}{nC} \ , \ \text{where Gain} = \frac{1 + nd_0}{1 - d_0} \tag{13}$$

The control-to-output transfer function of the series-connected coupled-inductor boost converter is derived and the resulting control-to-output transfer function is given below.

$$\frac{\Delta\overline{V_0}(s)}{\Delta d(s)} = \frac{V_o(1-d_0)}{(n+1)L_m.nC} \frac{\left(1 - s\frac{(1+nd_0)(n+1)L_m I_0}{(1-d_0)^2 V_0}\right)}{\left(s^2 + \left(\frac{d_0 r_{on}}{L_m} + \frac{(1-d_0) r_{off}}{(n+1)L_m}\right) s + \frac{(1-d_0)^2}{nC.(n+1)L_m}\right)} \tag{14}$$

The existence of the series-connected coupled inductor with turns ratio n changes both the system's dynamic behaviour and its gain compared to a regular boost converter. The numerator in (27) adds a zero, while the denominator is a second-order polynomial that shows the system's dynamic poles, which include both damping and natural frequency terms. The transfer function structure is like a normal second-order system with a zero in the right half-plane (RHP). It can limit the control bandwidth and phase margin.

b) Linearized Small-Signal Model of Parallel connected Coupled Inductor Boost Converter

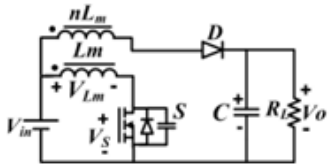

Fig. 8 Parallel connected coupled inductor boost converter

The ON and OFF circuit configurations of the parallel connected coupled inductor (CI) boost converter, which include parasitic elements, as illustrated in Fig.9.

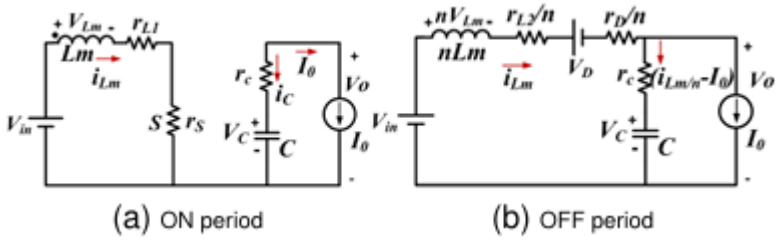

Fig. 9 ON and OFF periods of parallel connected coupled inductor boost converter

In a similar manner to the series-connected coupled-inductor converter, the state-space representation of the parallel-connected converter can now be expressed as follows:

$$\begin{bmatrix} \frac{d\overline{i_{Lm}}}{dt} \\ \frac{d\overline{v_C}}{dt} \end{bmatrix} = \begin{bmatrix} -\left(\frac{d_0 r_{on}}{L_m} + \frac{(1-d_0)r_{off}}{nL_m}\right) & -\frac{(1-d_0)}{nL_m} \\ \frac{(1-d_0)}{nC} & 0 \end{bmatrix} \begin{bmatrix} \overline{i_{Lm}} \\ \overline{v_C} \end{bmatrix} + \begin{bmatrix} \frac{d_0}{L_m} + \frac{1-d_0}{nL_m} & -\frac{(1-d_0)}{nL_m} & \frac{(1-d_0)r_C}{nL_m} \\ 0 & 0 & -\frac{1}{C} \end{bmatrix} \begin{bmatrix} \overline{v_{in}} \\ V_D \\ \overline{i_o} \end{bmatrix} \quad (15)$$

$$\bar{v}_o = \begin{bmatrix} (1-d_0)\frac{r_C}{n} & 1 \end{bmatrix} \begin{bmatrix} \overline{i_{Lm}} \\ \overline{v_C} \end{bmatrix} + \begin{bmatrix} 0 & 0 & -r_C \end{bmatrix} \begin{bmatrix} \overline{v_{in}} \\ V_D \\ \overline{i_o} \end{bmatrix} \quad (16)$$

The corresponding control-to-output transfer function for the parallel-connected coupled-inductor boost converter is given in (33).

$$\frac{\Delta\overline{V_0}(s)}{\Delta d(s)} = \frac{V_o(1-d_0)}{nL_m.nC} \frac{\left(1 - s\frac{(1+nd_0-d_0)nL_m I_0}{(1-d_0)^2 V_0}\right)}{\left(s^2 + \left(\frac{d_0 r_{on}}{L_m} + \frac{(1-d_0)r_{off}}{nL_m}\right)s + \frac{(1-d_0)^2}{nC.nL_m}\right)} \quad (17)$$

where $r_{on} = r_{L1} + r_s \ , \quad r_{off} = \frac{r_{L2}}{n} + \frac{r_D}{n} + \frac{r_C}{n}$

V. Results and Discussions

Table I lists the design parameters used for both converters.

Table I: Design Parameters

Specification	Symbol	Value
Output power	P_0	100 W
Input voltage	V_{in}	24 V
Turns ratio of coupled inductor	n	1
Steady-state duty cycle	d_0	0.5
Magnetizing inductance	Lm	40 µH
Output capacitance	C	40 µF
Primary winding resistance	r_{L1}	0.05Ω
Secondary winding resistance	r_{L2}	0.05Ω
Diode forward resistance	r_D	0.05Ω
Switch on-state resistance	r_S	0.05Ω

Figure 10 shows the open-loop responses of the mathematical models of the series- and parallel-connected coupled-inductor boost converters.

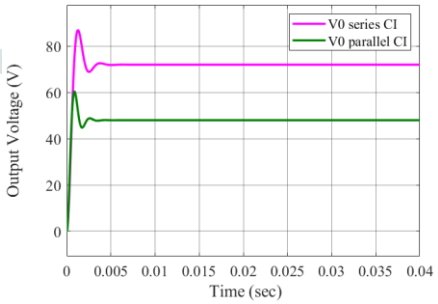

Fig. 10 Open-loop responses of the mathematical models

Figure 4 illustrates the open-loop output-voltage responses of the mathematical models for the series- and parallel-connected coupled-inductor boost converters. Starting from zero initial conditions, both converters exhibit a fast rise and a small transient overshoot before settling to their respective steady-state values. The series-connected topology converges to approximately 72 V, whereas the parallel-connected topology settles around 48 V, in accordance with the ideal voltage-gain expressions derived earlier. These results confirm that the series-connected converter provides a higher step-up ratio than the parallel-connected one under the same operating conditions and validates the analytical aspects.

V. CONCLUSIONS

This paper has presented the modelling and comparative analysis of series- and parallel-connected coupled-inductor boost converters. Simplified averaged state-space models and corresponding linearized small-signal representations were derived in a form analogous to the conventional boost converter, resulting in second-order control-oriented models for both topologies. These models explicitly incorporate the effect of the turns ratio and parasitic resistances, while remaining sufficiently simple for analytical study and controller design.

The open-loop responses of the mathematical models, shown in Fig. 4, confirm the expected steady-state behaviour: for identical design specifications and duty cycle, the series-connected converter settles at approximately 72 V, whereas the parallel-connected converter settles around 48 V. This agrees with the ideal gain expressions and clearly demonstrates the higher step-up capability of the series configuration. Both converters exhibit fast transient response with limited overshoot, indicating that the proposed models capture the dominant dynamics effectively.

From a comparative standpoint, the series-connected coupled-inductor boost converter is more suitable for applications requiring a higher voltage gain from the same input source, while the parallel-connected converter offers a lower output voltage but can be advantageous when reduced current stress and more moderate gain are sufficient. Overall, the developed models provide a useful basis for further work on closed-loop control, optimization, and hardware implementation of coupled-inductor high step-up converters in renewable energy and other DC-DC interface applications.

REFERENCES

[1] F. Mumtaz, N. Z. Yahaya, S. T. Meraj, B. Singh, R. Kannan, and O. Ibrahim, “Review on non-isolated DC–DC converters and their control techniques for renewable energy applications,” *Ain Shams Engineering Journal*, vol. 12, no. 4, pp. 3747–3763, 2021, doi: 10.1016/j.asej.2021.03.022.

[2] P. P. Gupta, G. I. Kishore, and R. K. Tripathi, “Non-isolated high step up in voltage DC–DC converter topology for renewable applications,” *Journal of Circuits, Systems and Computers*, vol. 30, no. 6, p. 2150093, 2021, doi: 10.1142/S0218126621500936.

[3] L. Schmitz, D. C. Martins and R. F. Coelho, "A Simple, Accurate Small-Signal Model of a Coupled-Inductor-Based DC-DC Converter Including the Leakage Inductance Effect," in *IEEE Transactions on Circuits and Systems II: Express Briefs*, vol. 68, no. 7, pp. 2533-2537, July 2021, doi: 10.1109/TCSII.2021.3061942.

[4] A. Ayachit and M. K. Kazimierczuk, “Averaged small-signal model of PWM DC-DC converters in CCM including switching power loss,” *IEEE Trans. Circuits Syst. II, Exp. Briefs*, vol. 66, no. 2, pp. 262–266, Feb. 2019.